Metal Oxalates as a CO₂ Solid State Reservoir: The Carbon Capture Reaction

Linda Pastero [1,2,*], Vittorio Barella [1], Enrico Allais [1], Marco Pazzi [3], Fabrizio Sordello [3], Quentin Wehrung [1] and Alessandro Pavese [1,2]
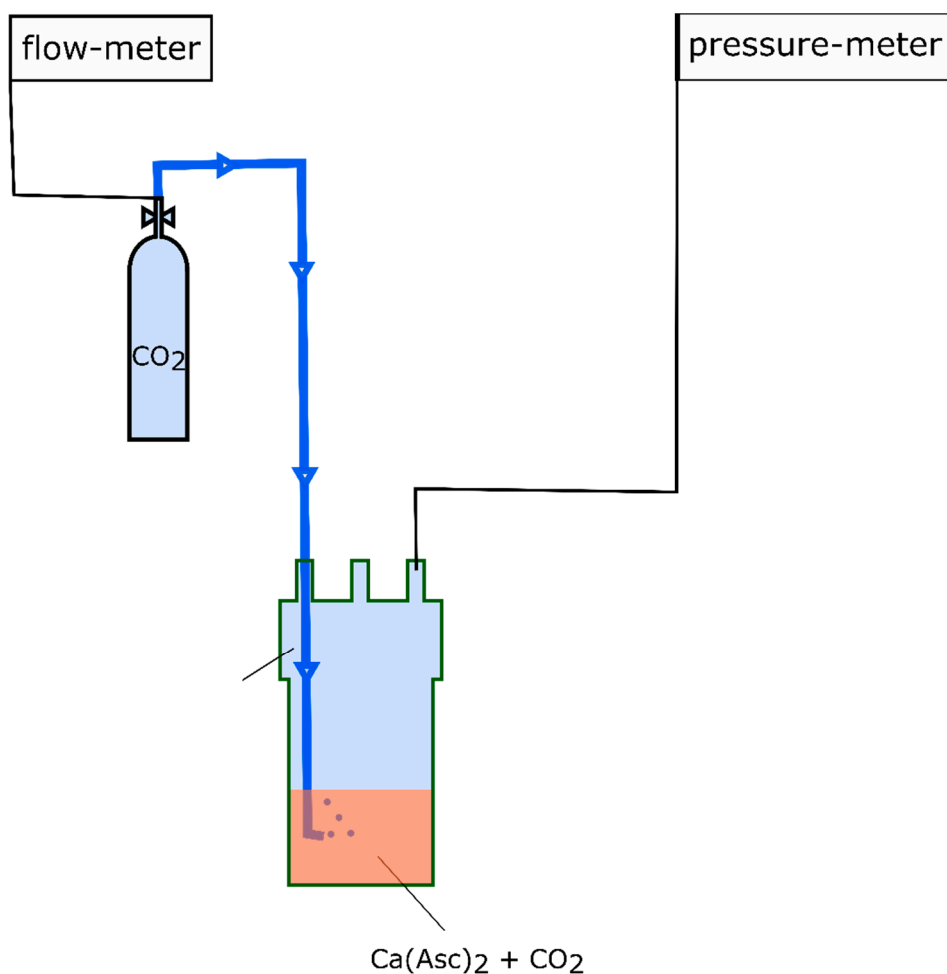
[1] Dipartimento di Scienze della Terra, Università degli Studi di Torino, Via Valperga Caluso 35, 10125 Torino, Italy; quentin.wehrung@unito.it (Q.W.); alessandro.pavese@unito.it (A.P.)

[2] NIS Interdepartmental Centre for Nanostructured Interfaces and Surfaces, Università degli Studi di Torino, Via Quarello 16, 10135 Torino, Italy

[3] Dipartimento di Chimica, Università degli Studi di Torino, Via Pietro Giuria 7, 10125 Torino, Italy; marco.pazzi@unito.it (M.P.); fabrizio.sordello@unito.it (F.S.)

*   Correspondence: linda.pastero@unito.it

Supplementary materials

flow-meter

pressure-meter

CO_2

$Ca(Asc)_2 + CO_2$

34

35 **Figure S1:** The B-setup. Carbon dioxide bubbles into the calcium ascorbate solution. The pressure setpoint is controlled

36 using a pressure-meter with a feedback loop on the flow-meter and it is chosen to be slightly higher than the atmospheric

37 pressure. After loading the system is closed and left to react.
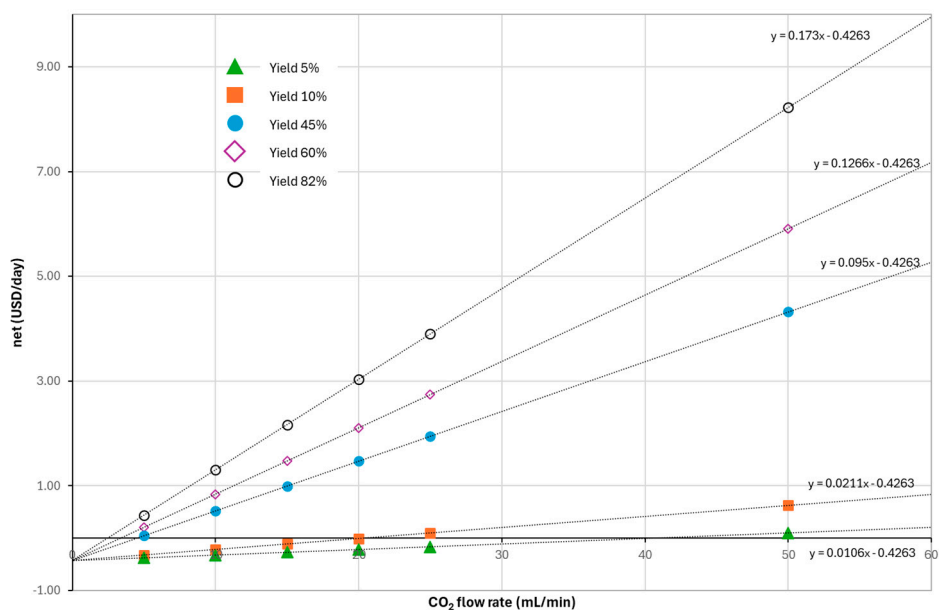
38

39

Figure S2: Flow rate vs net revenue at variable reaction yield. The model is built on the yields experimentally determined in our previous papers from laboratory setups [55,57]. Yields 5% and 45% are not experimentally determined and represent a hypothetical very low carbon capture performance (comparable to the average performance of B setup) and a cautionary average performance of a BD/SPRAY setup respectively. Prices of Ca[HA]$_2$ and Ca-oxalate: 750 USD/15kg and 600 USD/15kg respectively (data from retail market, May 2023). From the model we can infer the method is economically affordable for yields larger than 10% and CO_2 feeding equal or higher to 20 mL/min for a diluted Ca[HA]$_2$ solution (200mL, 0.1M)

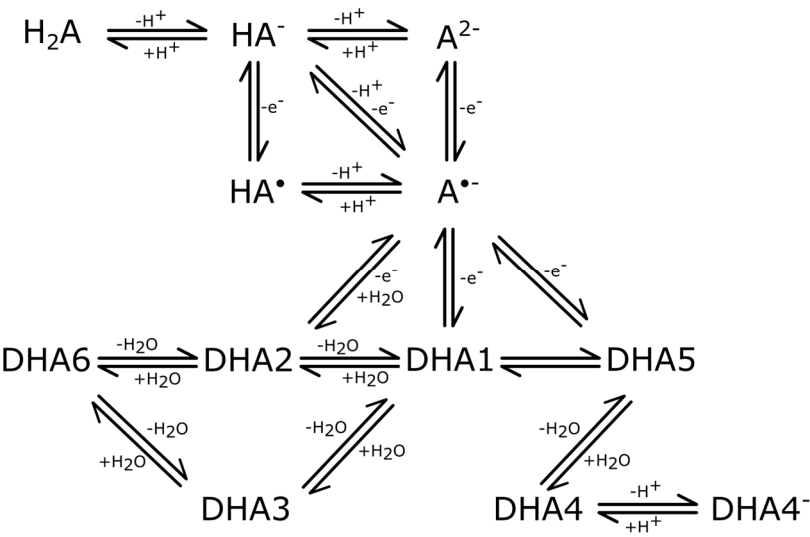| Reaction	Stage	pKa (experimental)	Red-Ox couple	E⁰ (V)
$H_2A - H^+ \leftrightarrow HA^-$	Reduced deprotonated	4.04^a		
$HA^- - H^+ \leftrightarrow A^{2-}$	Reduced deprotonated	11.34^a		
$HA^- - e^- \leftrightarrow HA^\bullet$	Oxidated 1st electron exchanged		$HA^-/ HA^\bullet$	$0.72V^c$; $0.766V^a$
$HA^\bullet - H^+ \leftrightarrow A^{-\bullet}$	Oxidated 1st electron exchanged	-0.45^b		
$HA^- - e^- - H^+ \leftrightarrow A^{-\bullet}$	Oxidated 1st electron exchanged			
$A^{2-} - e^- \leftrightarrow A^{-\bullet}$	Oxidated 1st electron exchanged		$A^{2-}/ A^{-\bullet}$	0.015V (pH=13.5); 0.085V (pH~11) ^{d}
$A^{-\bullet} - e^- + H_2O \leftrightarrow DHA2$	Oxidated 2nd electron exchanged			
$A^{-\bullet} - e^- \leftrightarrow DHA1$	Oxidated 2nd electron exchanged		$A^{-\bullet}/DHA1$	0.22V; 0.24V ^{e}
$A^{-\bullet} - e^- \leftrightarrow DHA5$	Oxidated 2nd electron exchanged			
$DHA2 - H_2O \leftrightarrow DHA1$	Oxidated 2nd electron exchanged			
$DHA1 \leftrightarrow DHA5$	Oxidated 2nd electron exchanged			
$DHA6 - H_2O \leftrightarrow DHA2$	Oxidated 2nd electron exchanged			
$DHA6 - H_2O \leftrightarrow DHA3$	Oxidated 2nd electron exchanged			
$DHA1 - H_2O \leftrightarrow DHA3$	Oxidated 2nd electron exchanged			
$DHA5 - H_2O \leftrightarrow DHA4$	Oxidated 2nd electron exchanged			
$DHA4 - H^+ \leftrightarrow DHA4^-$	Oxidated 2nd electron exchanged			

61

62 **Table S1:** Deprotonation and oxidation reactions following the model proposed by Tu et al. [74] see also Supporting

63 Information Fig.S2 for visual description of the reactions. pKa and E^0 values are reported as in the literature: a [75], b

64 [76], c [77], d [78], e [79].

65

66

Reduced (deprotonated) H_2A $\underset{+H^+}{\overset{-H^+}{\rightleftharpoons}}$ HA^- $\underset{+H^+}{\overset{-H^+}{\rightleftharpoons}}$ A^{2-}

Oxidized (1e⁻) $HA^\bullet$ $\underset{+H^+}{\overset{-H^+}{\rightleftharpoons}}$ $A^{\bullet-}$

Oxidized (2e⁻) $DHA6$ $\underset{+H_2O}{\overset{-H_2O}{\rightleftharpoons}}$ $DHA2$ $\underset{+H_2O}{\overset{-H_2O}{\rightleftharpoons}}$ $DHA1$ $\rightleftharpoons$ $DHA5$

                               $DHA3$ $DHA4$ $\underset{+H^+}{\overset{-H^+}{\rightleftharpoons}}$ $DHA4^-$

67

68   **Figure S3:** Scheme of the electrochemical equilibria of ascorbic acid and its derivatives in water solution. From Tu et al.,

69   modified [74]

Reaction	E⁰ (V)
$Cu^{2+} + 2e^- \leftrightarrow Cu$	0.337
$2NO_3^- + 6H_2O + 10e^- \leftrightarrow N_2 + 12OH^-$	0.252
$Cu^{2+} + e^- \leftrightarrow Cu^+$	0.153
$WO_4^{2-} + 8H^+ + 6e^- \leftrightarrow W + 4H_2O$	0.049
$Fe_2O_3 + 6H^+ + 6e^- \leftrightarrow 2Fe^+ + 3H_2O$	-0.051
$Fe_3O_4 + 8H^+ + 8e^- \leftrightarrow 3Fe + 4H_2O$	-0.085
$Sn(OH)_2 + 2H^+ + 2e^- \leftrightarrow Sn + 2H_2O$	-0.091
$SnO + 2H^+ + 2e^- \leftrightarrow Sn + H_2O$	-0.104
$SnO_2 + 4H^+ + 4e^- \leftrightarrow Sn + 2H_2O$	-0.106
$Pb^{2+} + 2e^- \leftrightarrow Pb$	-0.126
$Mn(OH)_3 + 3H^+ + 3e^- \leftrightarrow Mn + 3H_2O$	-0.157
$Ni^{2+} + 2e^- \leftrightarrow Ni$	-0.257
$Co^{2+} + 2e^- \leftrightarrow Co$	-0.28
$Cu_2O + H_2O + 2e^- \leftrightarrow 2Cu + 2OH^-$	-0.358
$H_2PO_4^- + 6H^+ + 5e^- \leftrightarrow P + 4H_2O$	-0.386
$Cd^{2+} + 2e^- \leftrightarrow Cd$	-0.403
$H_3PO_4 + 5H^+ + 5e^- \leftrightarrow P + 4H_2O$	-0.411
$ZnO + 2H^+ + 2e^- \leftrightarrow Zn + H_2O$	-0.439
$Fe^{2+} + 2e^- \leftrightarrow Fe$	-0.44
$Ga_2O_3 + 6H^+ + 6e^- \leftrightarrow 2Ga + 3H_2O$	-0.485
$V_2O_3 + 2H^+ + 2e^- \leftrightarrow V_2O_2 + H_2O$	-0.549
$Fe(OH)_3 + e^- \leftrightarrow Fe(OH)_2 + OH^-$	-0.56
$PbO + H_2O + 2e^- \leftrightarrow Pb + 2OH^-$	-0.58
$MnO + 2H^+ + 2e^- \leftrightarrow Mn + H_2O$	-0.652
$Zn^{2+} + 2e^- \leftrightarrow Zn$	-0.763

$Fe(OH)_2 + 2e^- \leftrightarrow Fe + 2OH^-$	-0.877
$Mn^{2+} + 2e^- \leftrightarrow Mn$	-1.180
$Mg^{2+} + 2e^- \leftrightarrow Mg$	-2.363

72

73　**Table S2:** The list of the metals with tabulated values of the redox potentials used to roughly evaluate the redox potential
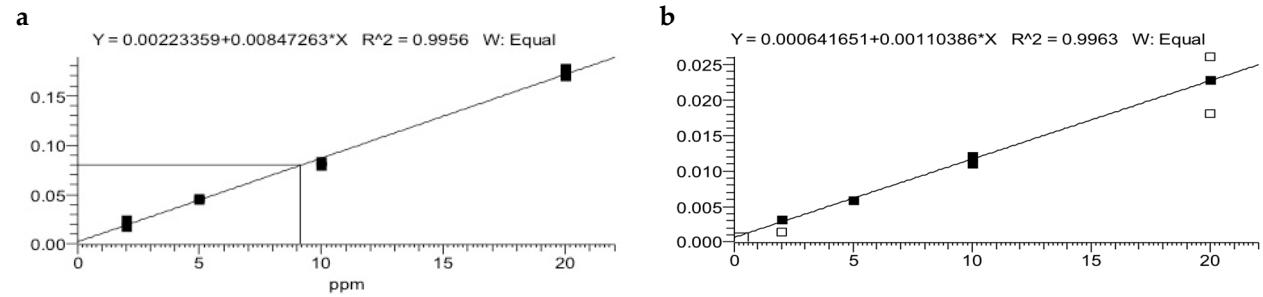
74　of a 1M aqueous ascorbic acid solution.

75

76

77

78

79

80

81

82

83

84　**Figure S4: a)** Calibration curve for H_2A, Calculated LOD e LOQ were respectively 0,48 and 1,6 ppm; b) Calibration curve

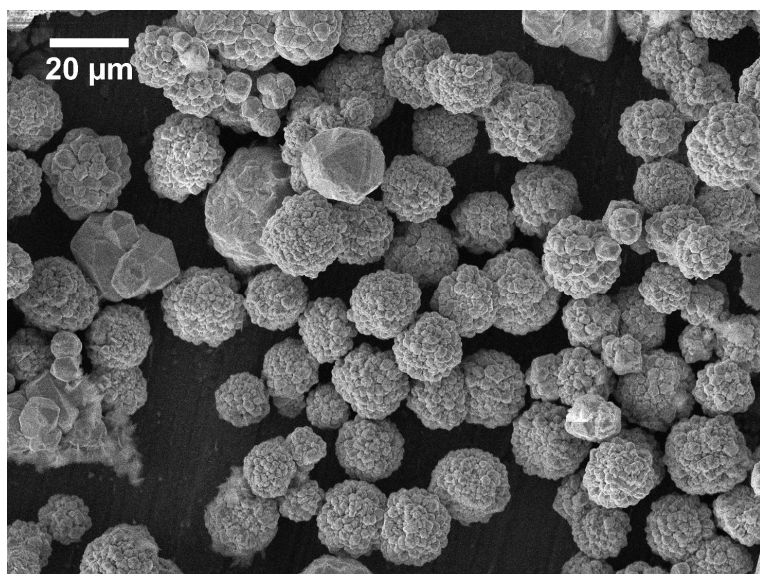85　for DHA Calculated LOD e LOQ were respectively 0,51 and 1,7 ppm.

86

87
88 **Figure S5:** Cu^0 crystals (single euhedral crystals and spherulitic aggregates) from the spontaneous redox reaction of CuO
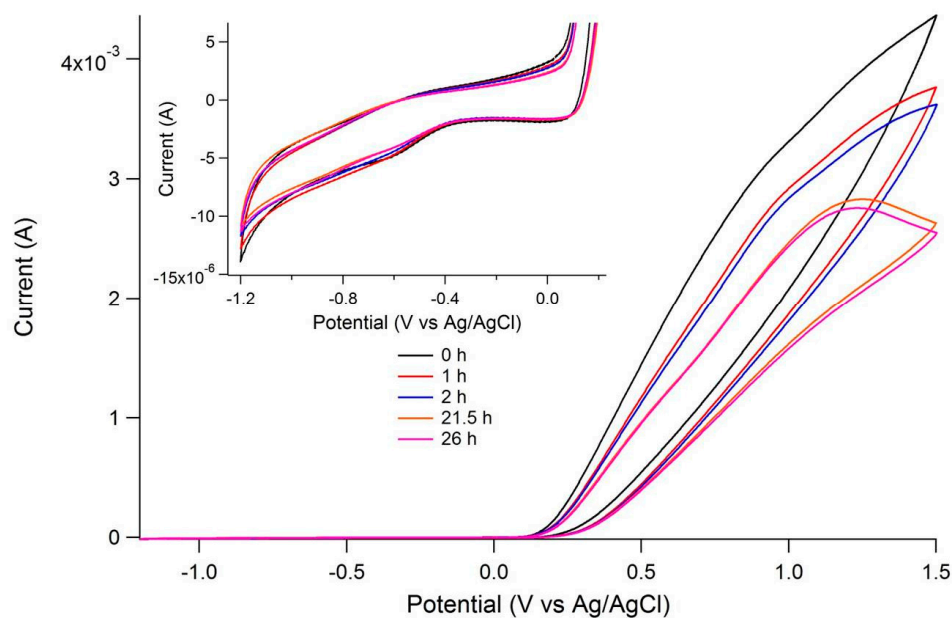89 with H_2A

90
91
92
93
94

95
96 **Figure S6:** Cyclic voltammogram at 50 mV/s scan rate of 1.0 M AA, 0.30 M $CaCl_2$ solution at pH 4.2 under CO_2 atmosphere.
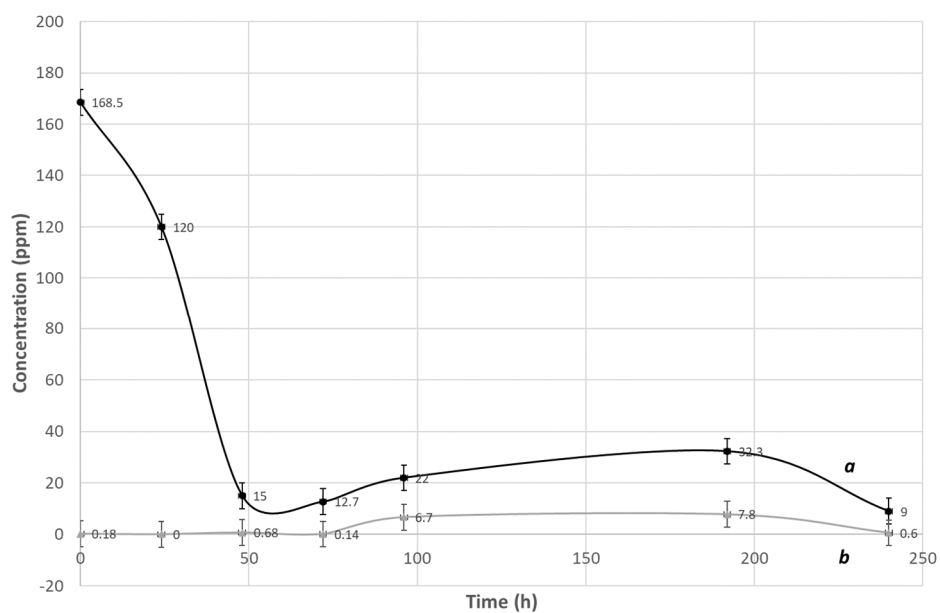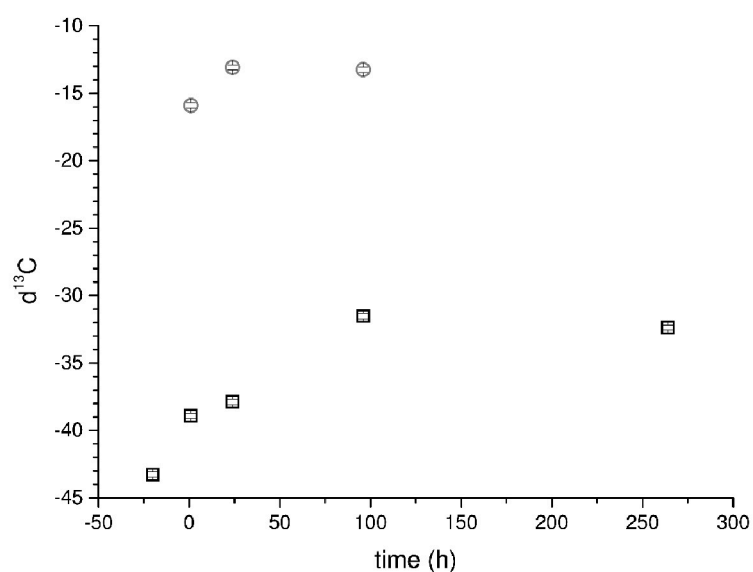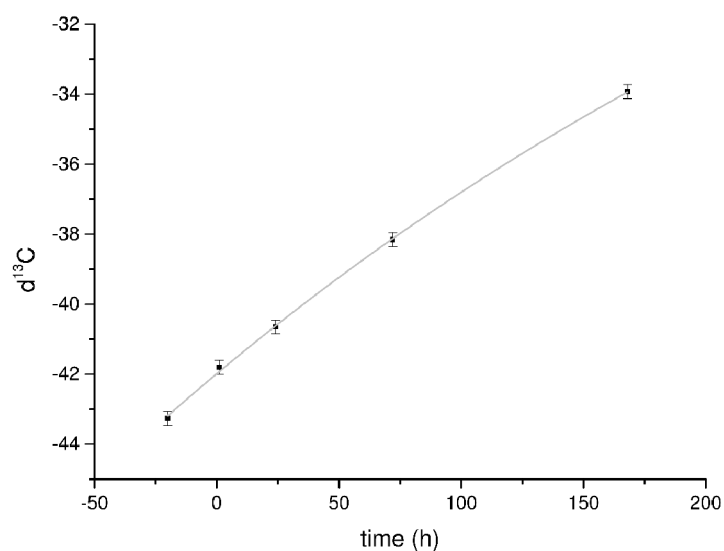
97

98

99 **Figure S7:** LC evaluation of the H₂A to DHA oxidation reaction. Curve **a**: H₂A concentration as a function of time; curve

100 **b**: DHA concentration as a function of time

101

102

103

104

105

106

107

108

	$d^{13}C$	$d^{18}O$
CO₂ canister	-43.26	-47.31
H₂A	-11.17	-9.62

109

110 **Table S3:** $d^{13}C$ and $d^{18}O$ ratios in the commercial CO₂ canister and the H₂A reagent
111

112

9

a

b

Figure S8: a) General ^{13}C enrichment trend for both the solid phase and the solution. Some artifacts affect values from the solution. The general trend is an enrichment of the ^{12}C in the gas fraction. Many crystal generations and zoning of crystals bring artifacts into the isotopic content of the solid phase. b) In the second experiment, we avoided the contamination from the air that could arise from the transfer of the solution from the reactor to the flasks. No sampling of the solid phase was performed until the end of the experiment. The single solid composition is averaged over the whole experiment time ($d^{13}C$ = -16.95).